

Warm Pressurant Gas Effects on the Static Bubble Point Pressure for Cryogenic LADs

Jason W. Hartwig¹, John B. McQuillen², David J. Chato³

NASA Glenn Research Center, Cleveland, OH, 44135, USA

This paper presents experimental results for the liquid hydrogen and nitrogen bubble point tests using warm pressurant gases conducted at the NASA Glenn Research Center. The purpose of the test series was to determine the effect of elevating the temperature of the pressurant gas on the performance of a liquid acquisition device (LAD). Three fine mesh screen samples (325x2300, 450x2750, 510x3600) were tested in liquid hydrogen and liquid nitrogen using cold and warm non-condensable (gaseous helium) and condensable (gaseous hydrogen or nitrogen) pressurization schemes. Gases were conditioned from 0K–90K above the liquid temperature. Results clearly indicate degradation in bubble point pressure using warm gas, with a greater reduction in performance using condensable over non-condensable pressurization. Degradation in the bubble point pressure is inversely proportional to screen porosity, as the coarsest mesh demonstrated the highest degradation. Results here have implication on both pressurization and LAD system design for all future cryogenic propulsion systems. A detailed review of historical heated gas tests is also presented for comparison to current results.

Nomenclature

d_{shute}	= Diameter of the shute wire [μm]
d_{warp}	= Diameter of the warp wire [μm]
D_p	= Effective pore diameter [μm]
g	= Gravitational acceleration [m/s^2]
HEX	= Heat exchanger
LL	= Liquid Level above LAD screen [m]
l_s	= Distance between consecutive shute wires [μm]
n_{shute}	= Number of shute wires per inch of screen [1/m]
n_{warp}	= Number of warp wires per inch of screen [1/m]
PCA	= Pressure control assembly
t	= Screen thickness [μm]
ΔP_{BP}	= Bubble point pressure [Pa]
ΔT	= Temperature difference between liquid and pressurant gas [K]
ε	= Porosity
γ	= Surface tension [mN/m]
ρ_{LH2}	= Liquid hydrogen density [kg/m^3]
θ_c	= Contact angle [degrees]

¹Research Aerospace Engineer, Propellants and Propulsion Branch, 21000 Brookpark Road, MS 301-3, Cleveland OH, 44135, Senior Member.

²Senior Aerospace Engineer, Fluid Physics and Transport Branch, 21000 Brookpark Road, MS 77-5, Cleveland, OH 44135.

³Senior Aerospace Engineer, Propellants and Propulsion Branch, 21000 Brookpark Road, MS 301-3, Cleveland, OH 44135, Associate Fellow.

I. Introduction

NASA maintains a strong desire to develop technology to enable long duration robotic and human space missions beyond Low Earth Orbit (LEO). Future destinations include Earth-Moon Lagrange points, near-Earth objects (NEOs) such as asteroids, and eventually surface missions to the Moon, Mars, and beyond. The development of new and existing propulsion capabilities to send robot and human afar is necessary for the exploration and study of these locations of interest. Due to significant increase in propulsion system performance compared to storable propellants (fluids that exist as liquids at room temperature), the advancement of cryogenic fluid propulsion systems remains at the forefront of NASA's technology development program.

Liquid oxygen/liquid hydrogen (LOX/LH₂) remains the top propellant combination owing to both an unmatched level of performance relative to other combinations, and due to proven flight heritage over the past 40 years in launch systems such as the Saturn V - S4, S4B, S2, Shuttle Space Transportation System (STS), short duration upper stages (J2). LOX/LH₂ systems also have potential usage for LEO fuel depots [1]. However there are challenging aspects when working with cryogenic propellants due to a low normal boiling point (NBP), low surface tension, and low viscosity. Cryogenic propellants are particularly susceptible to parasitic heat leak, which will make in-space storage and transfer a challenge.

II. Screen Channel Liquid Acquisition Devices

Technology development for LOX/LH₂ cryogenic propulsion systems begins upstream in the propellant tanks. Conceivably, there are two primary applications for in-space cryogenic liquid transfer, from the storage tank to the transfer line to an engine, or from a fuel depot to a customer spacecraft receiver tank. All cryogenic propulsion engines require vapor free liquid to be delivered to the injectors. Receiver depot tanks will also require very high liquid fill fractions due to the projected cost of launching and storing propellant in LEO in fuel depots. Single phase liquid acquisition in Earth's 1-g environment is straightforward, since gravity drives the heavier liquid to the bottom and lighter vapor to the top of the propellant tank. In microgravity conditions of LEO however, any one of a number of special propellant management devices (PMDs) are required to draw sufficient liquid to the tank outlet in varying thermal and gravitational environments. One type of PMD, a screen channel liquid acquisition device (LAD), relies on capillary flow and surface tension forces to acquire and maintain communication between the bulk liquid and tank outlet at all times. As shown in Fig. 1, screen channel LADs follow the contours of the tank walls. The side that faces the wall is covered with a fine mesh screen that wicks liquid into the channel and also blocks vapor ingestion during outflow if vapor is in contact with the screen.

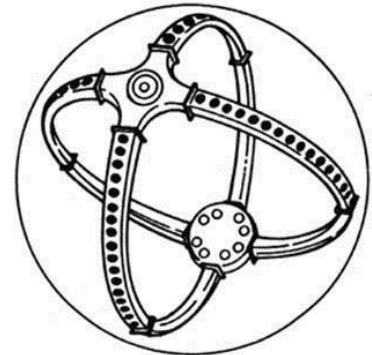


Fig. 1 Full Communication Screen Channel LAD

Screen channel LADs are characterized by the screen weave and mesh type, which refers to the number of wires per inch of material and type of pattern used during manufacture. For example, the 510x3600 screen is a Dutch Twill mesh with 510 warp wires and 3600 shuttle wires per square inch (20079 warp and 141732 shuttle wires per meter) of material as shown in Fig. 2. Each shuttle wire passes under two warp wires before going over the next warp wire, which creates a tortuous path to vapor ingestion. The screen selection is dictated by specific mission requirements, which include gravitational and thermal environments, and flow rate demands. Finer mesh screens are favorable for LH₂ systems to counter the low surface tension.

Screen channel LADs have proven flight heritage in storable propulsion systems such as the STS Reaction Control System (RCS) and Orbital Maneuvering System (OMS) [2 – 5], in cryogenic liquid helium (LHe) [6], but have not been used with LH₂ or LOX in low gravity. For flight systems, screen channel LADs are divided into two regimes [7, 8]. Start baskets or traps are small LADs that can be used in systems that experience large accelerations and large flow rates under short durations. Meanwhile full communication devices such as those

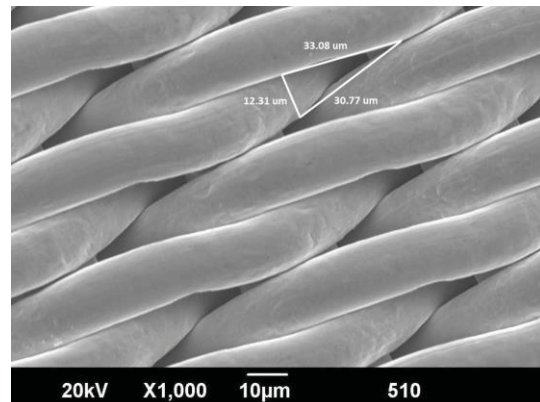


Fig. 2 Scanning Electron Microscopy Image of a 510x3600 Screen

depicted in Fig. 1 are used in systems with small accelerations and small flow rates under longer durations.

III. Pressurization System/LAD System Interaction

During spaceflight, there are two primary sources of heat leak into the tank as indicated by the red arrows in Fig. 3; one associated with storage and one with transfer of the propellant. Radiation and conduction heat leak enters the tank through the support struts, fill, vent, and instrumentation penetrations. Mitigation strategies to reduce heat leak are straightforward; passive thermal control is used to reduce heat leak by using thick multi-layer insulation (MLI) blankets, composite struts, and optimizing the MLI layer density, while active thermal control techniques use a cryocooler to reduce or eliminate propellant boil off. A second source of heat leak into the tank is from warm pressurant gas contacting the cold liquid propellant during liquid transfer. Mitigation strategies here are complicated. From a systems level standpoint, it is highly desirable to use warm gas as a pressurant because less mass is required to thermally condition the gas to tank conditions. From the LAD subsystem standpoint however, it is desirable to use cold gas because LADs are surface tension driven devices, and colder temperatures result in better performance.

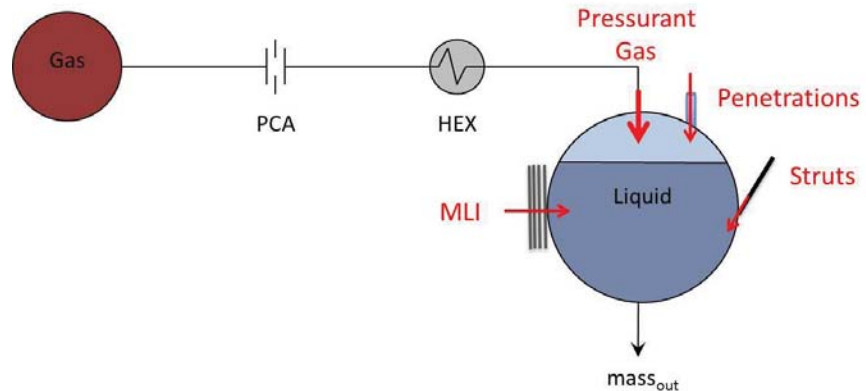


Fig. 3 Sources of Heat Leak into a Cryogenic Propellant Tank

During spaceflight, the pressurant gas typically assumes the environmental temperature, which is warmer than the saturation temperature for cryogenic propellants at atmospheric pressure. Even if the pressurant tank bottle is thermally linked to the propellant tank, the pressurant gas temperature will most likely be warmer than the liquid temperature. As will be shown later, warm pressurant will always decrease the surface tension of the cryogen, consequently, degrading the LAD performance. Clearly an optimal design point between the pressurization and LAD subsystems exists for each mission. In low gravity, warm gas may not impinge on the LAD screen until low tank fill levels, but tests are warranted to quantify the effect of heat absorption into the liquid on the LAD performance because warm gas will adversely affect the expulsion efficiency of the LAD.

In regard to the pressurization subsystem, there are two ways to pressurize a cryogenic propellant tank during liquid transfer. Autogenous pressurization utilizes the liquid's own vapor such as gaseous hydrogen (GH_2)/ LH_2 to pressurize while non-condensable pressurization employs a gas that will not condense into the liquid during pressurization. From a systems level standpoint, autogenous pressurization is more attractive due to overall lower system mass and potential reduced system complexity. However, this system may require heaters or pressure building circuits to maintain sufficient liquid flow rates. In addition, autogenous pressurization complicates liquid transfer due to added heat and mass transport across the LAD screen during outflow, which can prematurely warm the liquid and potentially cause the LAD to break down early. Therefore autogenous pressurization may be insufficient to sustain high outflow rates for prolonged periods of time. Meanwhile, pressurization with a non-condensable gas, such as helium, results in less heat and mass transfer at the LAD screen during outflow and also incurs less dissolution [9] in all major cryogenic propellants. Helium pressurization is likely sufficient to sustain all anticipated outflow rates [10]. However, non-condensable pressurization requires the use of onboard gas bottles as shown in Fig. 3, which increases overall system mass. In addition, GHe pressurization may be more expensive than autogenous pressurization because of the increasing cost of gaseous helium supplies. In a long duration depot mission GHe is a consumable resource which limits mission duration. Being able to generate pressurant (autogenous) eliminates issues associated with resupply of GHe.

IV. The Bubble Point Pressure

A screen channel LAD is said to have failed when vapor or gas is ingested into the channel, since the purpose of the LAD is to prevent gas ingestion into the channel. This failure or breakdown point is called the bubble point of the LAD screen. The bubble point is defined as the differential pressure across a LAD screen pore that overcomes the surface tension forces at that pore. Bubble point pressure is proportional to the surface tension of the liquid and inversely proportional to the effective screen pore diameter, as derived in Hartwig and Mann [11, 12] and shown in Eq. 1:

$$\Delta P_{BP} = \frac{4\gamma \cos \theta_c}{D_p(T)} \quad (1)$$

where γ is the surface tension of the fluid, θ_c is the contact angle, and D_p is the effective pore diameter. Vapor bubbles that penetrate into the channel may be condensed if conditions within the LAD are subcooled. However, helium bubbles that penetrate into the channel can only dissolve into the liquid, which is a very slow process, and could potentially cause engine instability.

The effective pore diameter is most readily determined through room temperature bubble point tests in a reference fluid such as isopropyl alcohol (IPA), which provides a good calibration range for low surface tension cryogenic liquids. Hartwig et al. [13] showed that the effective pore diameter is temperature dependent, and derived a simple pore diameter model to account for screen pore diameter shrinkage at colder temperatures to account for differences in bubble points for the same screen that could not be attributed to the fluid surface tension. Measurement of pore diameters using scanning electron microscopy (SEM) imaging has proven unreliable [14, 15]. In addition, there are inconsistencies about performance based on wire counts. For example, the 450x2750 mesh outperforms both the 325x2300 and 510x3600 meshes in room temperature and cryogenic liquids [14, 16]. However, the performance of the coarser 325 mesh surpasses the performance of the 510 mesh in room temperature liquids, but the opposite occurs in liquid nitrogen (LN₂) and LH₂. Note that Eq. 1 does not differentiate for pressurization gases. Previous experimental programs using cryogenic liquids, LH₂, LOX, and liquid methane (LCH₄) have demonstrated better performance when pressurizing with a non-condensable pressurant gas like GHe versus pressurization with a condensable gas such as GH₂ [14, 17 – 19, 20].

Screen channel LADS have flight heritage with storable propellants where heat transfer effects are not as severe as they are for cryogenic propellants. Before these LADs can be routinely used in cryogenic propulsion systems, the effects of undesirable heat on the LAD must be fully quantified. This environmental parasitic heat leak into the tank or heat input from warm pressurant gas may adversely affect LAD performance by vaporizing the liquid and drying out of the LAD screen. The static bubble point pressure is the upper limit on the total allowable pressure loss in a LAD system and therefore serves as the primary performance parameter for characterizing a screen channel LAD.

V. Test Objectives

Issues that arise in LH₂ cryogenic fluid management have been addressed through a battery of ground tests between FY11 – FY13 as part of the Cryogenic Propellant Storage and Transfer (CPST) technology maturation. Previous work has addressed the effect of varying the screen mesh, liquid, liquid temperature and pressure, and type of pressurization gas on the liquid hydrogen bubble point [13]. The purpose of this work was to examine the effect of warm pressurant gas on the bubble point of screen channel LADs. The goal is to give mission designers direct insight into the combined LAD and pressurization subsystem performance and design for future cryogenic engines and cryogenic fuel depots.

VI. Experimental Design

Testing was performed at the Cryogenic Components Lab 7 (CCL-7) at Glenn Research Center (GRC) in Cleveland, Ohio. Pore sizes for 325x2300 (12795 warp and 90551 shute wires per meter), 450x2750 (17716 warp and 108268 shute wires per m), and 510x3600 (20079 warp and 141732 shute wires per meter) Dutch Twill were determined in room temperature tests [11, 12]. The exact same samples were used here for heated pressurant gas tests in cryogenic liquids. LAD screen samples, 6.5 cm (2.5 in) in diameter, were cut and welded to a heavy flange to create a tight seal along the edges as shown in Fig. 4. Each screen was mounted to its own flange to permit rapid change out. The screen was mated with a cylindrical cup shown in Fig. 5. The purpose of the cup was to create the liquid/vapor interface (L/V) within the screen pores by pressurizing from beneath the screen for the inverted bubble point (IBP) test configuration. The cup was equipped with a central support rod as shown in Fig. 6. The rod had a custom fabricated cross to allow for slow, uniform pressurant gas injection into the cup. The rod also supported three annular thin film Kapton heaters which warmed the incoming pressurant gas to the desired temperature before

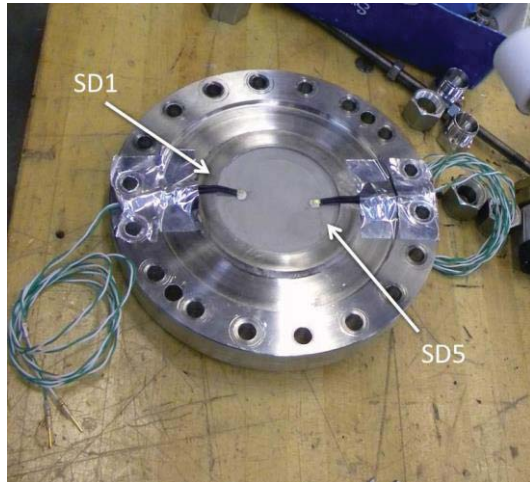


Fig. 4 LAD Screen Sample and Flange



Fig. 5 LAD Cup

gradually increase due to parasitic heat leak into the dewar and through introduction of the warm pressurant gas. The liquid was evaporatively cooled by reducing pressure within the dewar. Temperature of the pressurant gas was monitored using a silicon diode inside the LAD cup and controlled by cycling on or off the heaters, which were controlled through a tight PID loop using a silicon diode inside the LAD cup.

All temperatures were measured using silicon diodes as point sensors. Critical measurements for heated pressurant gas tests were the temperature of the liquid and gas side of the LAD screen, temperature of the pressurant gas, pressure of the ullage, DPT across the LAD screen, and pressurant gas mass flow rates into the cup. All data was recorded at 5 Hz with a computer data acquisition system (DAQ). Videos of the LAD screens were time stamped and recorded to compare with the time stamp in the data. All diodes measured temperature to within 0.1 K. Ullage pressure was measured to within 2.3 kPa accuracy. The raw DPT reading was accurate to within 0.324 Pa, but due to signal interpretation and processing, video read off errors, interpolation between recorded values, the total uncertainty in the corrected bubble point pressure is estimated to be 12 Pa, which is 10% uncertainty in the lowest reported bubble point pressure for the heated gas runs. This low absolute error in measurement relative to previously reported cold gas tests was made possible by modifications in the DAQ system.

Experimental methodology and the original test matrix are outlined in previous work [16]. To conduct a heated pressurant gas bubble point test, a GHe flow was first established across the

incidence on the LAD screen. A heater was placed on the underside of the bottom and top disc, and the top of the bottom disc, which eliminated view factors between heating source and LAD screen, and ensured that all of the heating was via conduction and convection of the incoming pressurant gas. This design forced uniform heating and pressure rise within the cup. It also eliminated direct warm gas impingement on the screen. Bubble point pressure was deduced from the raw differential pressure transducer (DPT) measurement from the sense line shown in Fig. 5. The sensing port pointed away from the screen to eliminate flooding of the line and to eliminate two phase DPT signals. The complete assembled LAD screen and cup is shown in Fig. 7.

The LAD screen and cup assembly was placed in a dewar. The purpose of the dewar was to house the liquid cryogen on top of the LAD screen. A polished aluminum plate was mounted above the screen and cup assembly and reflected an image of the LAD screen through a viewport on the side of the dewar to a camera. A fiber optic light source illuminated the screen. A camera was attached to the side viewport to monitor the test in real time. Time synchronization between camera and data was maintained through a custom time synchronization system. Facility air ejectors were used to control pressure and thus temperature of the liquid. The facility was modified to use GHe and GH_2 as pressurants for LH_2 testing and GHe and gaseous nitrogen (GN_2) as pressurants for LN_2 tests.

Pressure in the dewar was controlled by a proportional-integral-derivative (PID) loop. Liquid temperature was controlled by conditioning the liquid in storage dewars that were connected to the facility. Liquid temperature would



Fig. 6 Heater Bank

screen during liquid fill of the dewar to prevent flooding of the cup. Heated pressurant gas testing was always conducted in above atmospheric pressure conditions, which eliminated the need to pre-condition the liquid. The liquid temperature only varied between a small range of 20.5 K – 21.0 K, which allowed independent examination of the effect of heated pressurant gas on LAD performance. When the dewar was filled to the desired liquid level, the pressurant gas type was selected and allowed to flow through the flow network for a period of 10 minutes or more. The screen was then allowed to reseal. The heaters were then engaged until the desired temperature of the pressurant gas was achieved. The gas was always allowed several minutes residence time to come to equilibrium at the desired gas temperature before attempting a controlled breakthrough. Then the pressure underneath the LAD screen was slowly increased until a bubble broke through the wetted screen as indicated on the live video and in the sharp rise in the DPT signal. The screen was then resealed. Bubble points were repeated at similar pressurant gas temperatures for repeatability before moving on to the next gas temperature. Due to the low surface tension of LH₂ and low baseline cold gas bubble point values, it was sometimes difficult during testing to even reseal the screens. Raw bubble point pressures were corrected for liquid head pressure:



Fig. 7 Completed LAD Screen/Cup Assembly

$$\Delta P_{BP}(T, P)|_{\text{exp}} = DPT - \rho_{LH_2} gLL \quad (2)$$

where LL was the liquid level above the screen in the dewar as determined by a vertical silicon diode rake.

The test matrix consisted of the following: Three fine mesh screen channel LAD samples (325x2300, 450x2750, and 510x3600) were tested in two cryogenic liquids (LH₂ and LN₂), with two pressurization schemes (condensable GH₂/LH₂ and GN₂/LN₂ and non-condensable GHe/LH₂ and GHe/LN₂) at several different pressurant gas temperatures. Bubble point data was first collected using cold pressurant gases. The cold baseline temperature of 20.3K was approximately equal to the liquid temperature to minimize the temperature gradient across the screen at breakdown. This was only possible because the LAD cup was immersed in the liquid. To collect data at elevated temperatures, the heaters were engaged to several different fixed gas temperatures and measurements repeated to allow comparison with the cold gas data using Eq. 2.

VII. Liquid Hydrogen Tests

Using the current hardware and test configuration, parametric testing was conducted to independently examine the effect of six different parameters on the bubble point pressure. The parameters included screen weave, liquid (surface tension), liquid temperature and pressure, pressurization gas type, and pressurization gas temperature. Results from testing with cold gas [13] are used to establish the baseline reference bubble point values. Bubble point is directly proportional to the surface tension of the liquid in Eq. 1. The pressure dependence on bubble point is believed to be a modification of the temperature dependence [19, 20]. Higher pressures relative to the saturation pressure, and thus higher levels of liquid subcooling at the screen, produced higher bubble points for previously reported LOX and LCH₄ data.

Figure 8 establishes the effect of changing the screen weave, liquid temperature and pressure, and pressurization gas type on the LH₂ bubble point pressure by plotting data for all three screen meshes and both pressurant gases. The trends are as follows: First, for all three meshes, and for both pressurant gases, bubble point decreases with increasing liquid temperature, due to decreasing surface tension. The highest bubble point pressures are always obtained in the coldest liquid temperatures, regardless of screen or gas type. Second, for all three meshes, regardless of liquid temperature, bubble points obtained using the non-condensable gas are always higher than those obtained using the condensable gas. Gaseous helium adds margin to the bubble point pressure while GH₂ acts like a degradation factor. The disparity between pressurization schemes is relatively fixed for all three LAD screen meshes tested here. Third, for all liquid temperatures and for both pressurant gases, bubble point pressure does not scale with the mesh of the screen. This is the most complex trend of the original five parameters tested [14]. The second finest 450x2750 mesh produced the highest bubble points, for both GHe and GH₂. The 510x3600 mesh outperformed the 325x2300 mesh at LH₂ temperatures, but the 325x2300 yielded higher pressures in room temperature liquids [11, 12]. The reason for this crossover in performance is due to the temperature dependence of the screen pore diameter, as mentioned previously. In addition, the controlling parameter for gain in performance

with reduced temperature is the shute to warp diameter ratio [21]. The geometry of the L/V interface at breakthrough is dependent on this ratio, and as previously shown, the 510 screen has the largest gain at LH₂ temperatures.

The sixth and final parameter that was investigated was the temperature of the pressurant gas. Data is first presented on an absolute scale to allow direct comparison to cold gas data. Figure 9 plots all LH₂ bubble point data collected using warm pressurant gas. Data is plotted as a function of the temperature difference between warm gas and cold liquid at breakthrough. Controlled breakthroughs and reseals were achieved for gas temperatures between 30K < T_{GAS} < 116K which correspond to a temperature difference across the screen of 10K < ΔT < 95K. As shown for all three screens, the bubble point pressure decreases linearly with increasing pressurant gas temperature. The degradation in bubble point is more pronounced using GH₂ vs. pressurizing with GHe as the 325x2300 and 450x2750 screens failed to reseal at temperature differences of 34K and 69K, respectively using the condensable gas. Meanwhile, controlled breakthroughs were achieved with all three meshes using GHe beyond temperature differences of 50K. Regardless of the pressurization method, the onset of degradation is immediate for gas temperatures greater than the liquid temperature. This is in contrast to previously reported LH₂ heated gas bubble point pressures where the onset of degradation would occur at a certain gas temperature.

To allow comparison between the four different LAD test methods in Appendix A, a normalized bubble point ratio is defined:

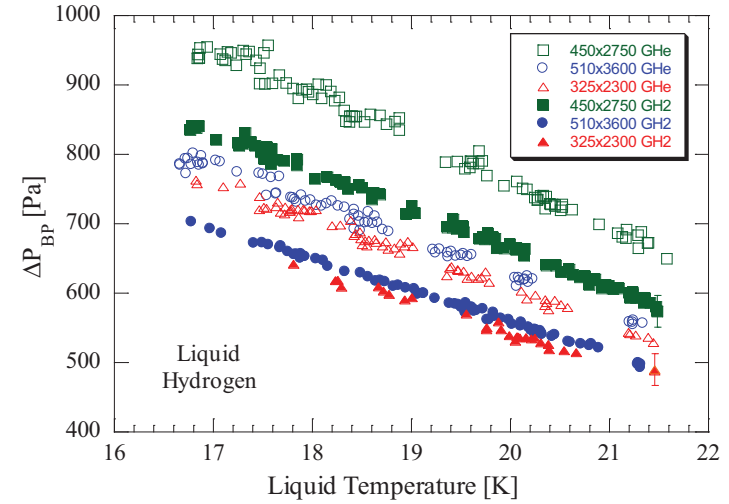


Fig. 8 Cold Gas Liquid Hydrogen Bubble Point as a Function of Liquid Screen Side Temperature.

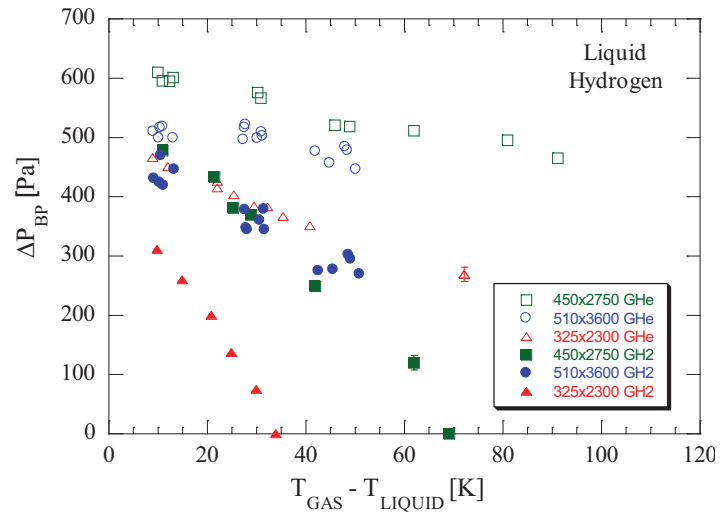


Fig. 9 Heated Pressurant Gas LH₂ Bubble Point as a Function of Temperature Difference between Pressurant Gas and Liquid.

$$\frac{\Delta P_{BP}(\Delta T)}{\Delta P_{BP}(\Delta T = 0)} \quad (3)$$

where ΔT is the temperature difference between liquid propellant and pressurization gas. Therefore the denominator is the normal breakdown value for equal gas and liquid temperatures, and the numerator is the breakdown value when the gas is sufficiently heated above the liquid temperature (i.e. the temperature difference across the screen). The normalized ratio is plotted as a function of the temperature difference across the screen.

Figure 10 plots heated bubble point pressures using Eq. 3 to normalize the data to the cold gas value obtained at the liquid temperature. Since each controlled breakthrough/reseal pair occurred at different liquid temperatures spaced over an approximate temperature range of 21 K < T < 22 K, each point was normalized to its own cold gas bubble point pressure, as opposed to a single value. Therefore, at a temperature difference across the screen of 0K, there is no deviation from the unheated pressurant gas bubble point ratio, by definition. Data is again plotted as a function of the ΔT across the screen. Lines are simple linear fits to the data.

Normalizing the data shows three distinct trends. First, for all 3 screens and both pressurant gases, heating the gas above the liquid temperature acts as a degradation factor on the cold gas bubble point pressure. The larger the temperature difference across the screen, the earlier the screen will break down. Second, for all three screens, bubble point pressure degrades from the cold gas value much more rapidly using condensable gas than using non-condensable gas as indicated by steeper slopes in the linear curve fits. Third, for both pressurization schemes, degradation in bubble point is inversely proportional to the porosity of the screen. Porosity is the ratio of open area for fluid to flow through the screen divided by the total screen area. Porosity for the LAD screens is defined as:

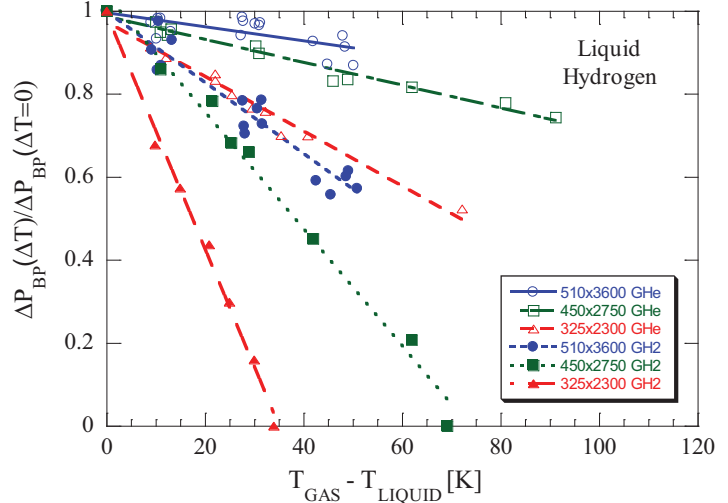


Fig. 10 Normalized Heated Pressurant Gas LH₂ Bubble Point Pressure as a Function of the Temperature Difference between Pressurant Gas and Liquid at the LAD Screen.

$$\varepsilon = 1 - \frac{\pi}{4} (n_w d_w^2 + 0.5 n_s d_s^2 + 0.5 n_w n_s d_s^2 l_s) \quad (4)$$

where n_w and n_s are the number of warp and shute wires per inch of screen material, respectively, d_w and d_s are the diameters of the warp and shute wires, and l_s is the distance between consecutive shute wires as defined by [22]:

$$l_s = \sqrt{(d_w + d_s)^2 + \left(\frac{1}{n_w}\right)^2} \quad (5)$$

Computed screen thicknesses and porosities are shown in Table 1. Therefore higher porosities indicate more open area for the gas to interact directly with the liquid. As shown in Fig. 10, the finest 510x3600 mesh exhibited the smallest degradation in performance over the 450x2750 and 325x2300 screen, as indicated by the slopes of the linear curve fits. This trend holds for both pressurization schemes. As is evident in Figs. 9 and 10, although the 450x2750 screen outperforms the 510x3600 on an absolute basis, degradation in performance for the 510x3600 screen is less.

Screen	Screen Thickness [μm]	l_s [μm]	ε
325x2300	88.9	100.7	0.245
450x2750	66	72.8	0.267
510x3600	56.4	65.0	0.284

Table 1 – Calculated Screen Parameters

Coarser screens are likely to sustain higher temperature differences across the screen prior to bubble breakthrough, causing the local interfacial temperature to increase significantly higher than finer meshes. For Dutch Twill screens, the screen thickness for a heated gas bubble to traverse from gas to liquid side of the screen is approximately equal to:

$$t = (2 * d_{shute}) + d_{warp} \quad (6)$$

Therefore coarser Dutch Twills are thicker and have lower porosities relative to finer Dutch Twills. These longer path lengths for warm gas or vapor to travel through the screen coupled with less overall open area for gas and liquid

to exchange heat and mass causes larger temperature differences to build across the screen before the actual visible warm gas bubble breaks through the screen. The finest 510 mesh is the thinnest screen and has the smallest pores, and largest porosity, making it easier for heat and mass to transport across the screen between liquid and gas prior to breakdown. Since mass is more easily transferrable across the screen, the local gas at the screen pore will cool slightly, cooling the interface temperature relative to the coarser meshes long before the bubble breaks through the screen. Meanwhile, for the coarser mesh, the larger pore size, thicker screen, and lower porosity causes larger temperature differences across the screen to build prior to breakdown. The larger pore sizes and less contact area between warm gas and cold liquid prevent heat transfer from the gas into the liquid.

Data shows that coarser screens like 200x1400 and 325x2300 have larger temperature differences across the screen at breakdown [23]. The dominate mode of heat transfer for the finer mesh screens is primarily parallel path heat conduction: conduction within the metal and conduction within the liquid phase trapped initially in the mesh. Except at breakthrough, there is little convective motion through the screen as the tiny pore size and the liquid viscosity limit the motion.

The degradation in performance using condensable gas can also be explained as follows: As warm condensable vapor passes through the screen, it condenses into the liquid, and warms the L/V interface, reducing the surface tension and thus bubble point. For GHe pressurization, the small additional margin in bubble point pressure is due to the suppression of the local partial pressure of GH_2 within the screen pores. Free mass transport is minimized with helium present, but heat conduction between warm gas and cold liquid still occurs at a slightly lower rate relative to GH_2 pressurization. Messerole and Jones [24] speculated that for GH_2 pressurization, the liquid may be in a locally superheated state at the screen, which may cause any heat input into the liquid to produce bubbles immediately and lead to the liquid detaching from the screen. Meanwhile, for GHe pressurization, the liquid at the screen may be in a slightly subcooled state, since GHe has been shown to evaporate liquid away from the screen [19, 20].

Results are in fair agreement with Cady's [25] previously reported non-inverted bubble point (NIBP) results using a 325x2300 mesh and GHe; he showed a smaller degradation factor (despite higher heat transfer rates) of only 10% at a gas temperature 55K above the liquid temperature. However, Cady also reported near identical degradation in performance for several different meshes, which is in disagreement with the current study. The current study is also in agreement with Burge and Blackmon's [7] heated GH_2 NIBP data for a 250x1370 that showed steeper degradation relative to the 325x2300 GH_2 here. Note that the 250x1370 screen has a lower porosity relative to the 325x2300 and would be expected to degrade more relative to the finer meshes.

VIII. Liquid Nitrogen Tests

Heated pressurant gas tests were also conducted in LN_2 using the same exact screens, experimental design, and procedure. Only the DPT that was used to measure raw bubble point pressure was changed to a higher range DPT to account for the higher LN_2 surface tension, and thus bubble point, relative to LH_2 . Results are plotted in Figs. 11 – 13. First, the cold pressurant gas bubble point pressure as a function of the liquid screen side temperature is plotted to establish the baseline reference value. The same trends visible in LH_2 data are reflected in the LN_2 data in Fig. 11. For all three meshes and both pressurant gases, LN_2 bubble point pressure decreases with increasing liquid temperature. For all temperatures and meshes tested, pressurization with the non-condensable GHe yields higher performance over pressurization with the condensable GN_2 . For both pressurant gases and all liquid temperatures tested, the same trend between screen meshes is evident with LN_2 as in LH_2 tests. The second finest 450x2750 yields the highest bubble points, followed by the finest 510x3600 screen, followed by the coarsest 325x2300 mesh.

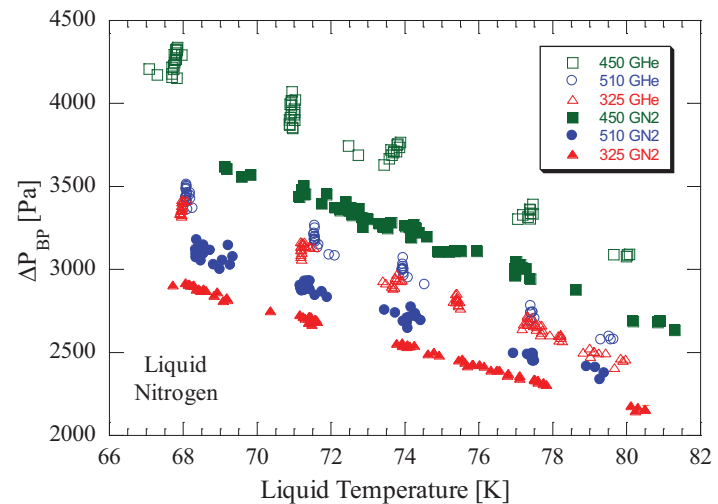


Fig. 11 Cold Gas Liquid Nitrogen Bubble Point as a Function of Liquid Screen Side Temperature. All data was taken at a pressurant gas temperature approximately equal to the liquid temperature.

Figure 12 plots heated pressurant gas bubble point data, on an absolute scale, as a function of the temperature difference across the screen at breakthrough. The liquid temperature for all of these tests was between the range of $79\text{K} < T_{\text{liquid}} < 81\text{K}$. Controlled breakthroughs were achieved for gas temperatures between $80\text{K} < T_{\text{GAS}} < 211\text{K}$ which correspond to a temperature difference across the screen of $1\text{K} < \Delta T < 131\text{K}$. Higher gas temperatures using GHe and GN₂ in LN₂ were achieved due to greater temperature stability of the LN₂ during testing; more controlled breakthroughs and reseals were achievable due to the higher LN₂ surface tension. As shown for all three screens, bubble point pressure decreases with increasing pressurant gas temperature. The degradation is again more pronounced using the condensable gas versus the GHe case. However, examination of Fig. 12 shows that the slopes in degradation for LN₂ are not as sharp as those for LH₂. In addition, for the 450x2750 and 510x3600 screens using GHe pressurization, the onset of degradation does not occur immediately.

To elucidate this apparent trend, Fig. 13 plots heated bubble point pressures using Eq. 3 to normalize the data to each cold gas bubble point value. Data is plotted as a function of the ΔT across the screen. Lines are fits to the data from the onset of degradation. The same trends in previous LH₂ data are reflected here in LN₂. Warmer pressurant gas temperatures degrade the bubble point ratio. Bubble point pressures degrade quicker using GN₂ over GHe pressurization as indicated by the steeper rate slopes. Degradation in bubble point is again inversely proportional to the porosity of the screen for both pressurization schemes. However, unlike LH₂ results, where the onset of degradation occurred immediately, onset of degradation in performance for the 450x2750 using GHe and 510x3600 using both GHe and GN₂ does not occur until a minimum temperature difference is achieved (41K, 77K, 21K, respectively). Compared to historical NIBP results from Castle [26], no degradation in performance was noticed for any of the fine Dutch Twill screens, including the 200x1400, 325x2300, or 450x2750 screens over a much larger temperature range using GN₂ pressurant.

LN₂ bubble points degrade less than LH₂ over the same range of ΔT . This could be due to the fact that LN₂ has a higher surface tension and higher heat capacity relative to LH₂, making it harder to alter the effective interfacial temperature and thus surface tension of the liquid at the screen pore. Castle [26] claimed that differences in degradation between LH₂ and LN₂ are because LH₂ is more susceptible to drying out because of the lower superheat required to initiate boiling. Differences could also be due to a stronger change in surface tension with temperature for hydrogen over nitrogen.

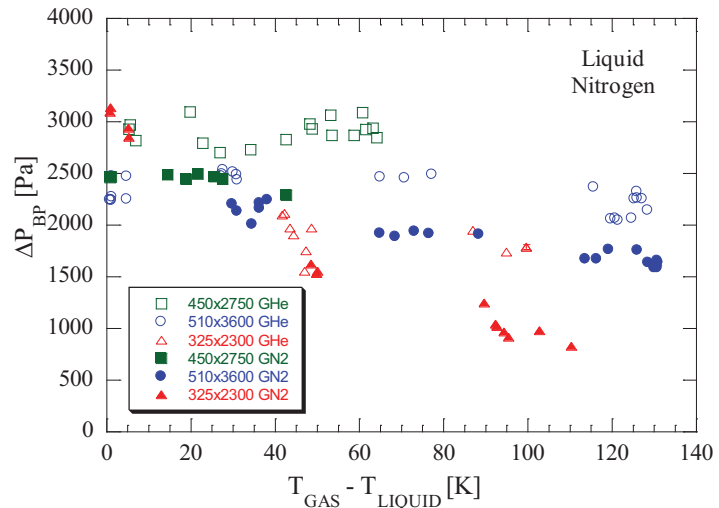


Fig. 12 Heated Pressurant Gas LN₂ Bubble Point as a Function of Temperature Difference between Pressurant Gas and Liquid.

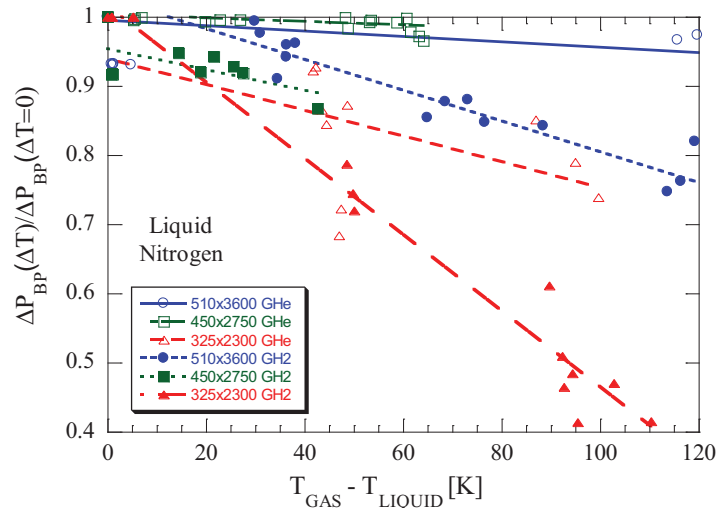


Fig. 13 Normalized Heated Pressurant Gas LN₂ Bubble Point Pressure as a Function of the Temperature Difference between Pressurant Gas and Liquid at the LAD Screen.

IX. Conclusion

Experimental results here confirm that elevating the pressurant gas temperature above the liquid temperature always acts as a degradation factor on the performance of the LAD. Three fine mesh screen channel LAD samples were tested in LH₂ and LN₂ using heated non-condensable (GHe) and condensable (GH₂/LH₂ or GN₂/LN₂) gases for temperature difference between the pressurant and liquid of 0 – 91K and 0 – 131K for LH₂ and LN₂, respectively. For all three meshes, both liquids, and both pressurization schemes, normalized bubble point pressure ratio decreases linearly with increasing gas temperatures. Degradation in performance is much sharper using condensable gases versus using non-condensable gases. The reduction in LAD performance scales inversely with the porosity of the screen for both liquids and pressurization schemes, as the finest 510x3600 mesh exhibited the least amount of degradation, and the coarsest 325x2300 mesh had the highest reduction in performance. For heated LH₂ bubble point tests, the onset of degradation always occurred immediately with warm gas for all three meshes, whereas for heated LN₂ tests, the onset of degradation did not occur below a minimum temperature difference between the pressurant gas and liquid for the 450x2750 and 510x3600 meshes.

Differences in performance between the three different screens are due to the effect of the screen thickness and porosity on the overall heat transfer across the LAD screen. Differences in performance between pressurants are due to modified heat and mass transport at the screen pore L/V interface through evaporation (GHe) and/or condensation (GH₂ or GN₂). Differences in performances between the two liquids have been explained through the differences in superheats required to initiate boiling in the liquid.

Results here have direct impact on future LAD and pressurization system design for low surface tension liquids, especially for future cryogenic hydrogen fueled depots. The bubble point pressure of screen channel liquid acquisition devices represents the upper limit on the total allowable pressure loss, and thus flow rate from the LAD to a transfer line en route to an engine or receiver depot tank. Higher bubble points are always obtained when the gas used to pressurize the propellant tank, and thus flow liquid through the LAD, is as cold as possible relative to the liquid, with the highest values obtained when the pressurant gas and liquid temperature are approximately equal. However, unless the pressurant gas bottles and propellant tanks are thermally linked, or subsurface pressurization methods are employed, the gas will always be significantly warmer than the cryogenic propellant and some degradation in LAD performance will be expected for all real mission scenarios. This work quantifies this effect.

Acknowledgments

This work was funded by the Cryogenic Propellant Storage and Transfer Project under the Office of the Chief Technologist at NASA. The authors would like to thank the operations team and research support staff at CCL-7 for their assistance during planning, design, and testing phases.

Appendix A – Previously Reported Experiments

There are four ways to experimentally test LAD performance. The easiest and most straightforward method to characterize the limits for a screen channel LAD is to measure the bubble point of a small screen sample. The method using an inverted bubble point (IBP), with liquid on top and vapor or gas on the bottom, is preferable over the non-inverted bubble point (NIBP) method for the following reasons: It is easier to control liquid head pressure on the submerged LAD screen sample, it is easier to deduce breakthrough pressures, and bubbles that break through the screen naturally rise away from the screen during breakthrough. A third method for testing LAD performance involves flowing liquid through a complete LAD channel assembly until the screen breaks down and vapor is ingested into the channel. Static IBP or NIBP tests are preferred over dynamic inverted outflow (IO) tests because IO test results can vary based on how the tank was pressurized, how the gas impinges on the screen (ex. parallel vs. perpendicular to screen face), and due to nonuniform pressurant gas temperature gradients which may develop during outflow. A fourth method for testing LAD performance is similar to the bubble point testing and involves immersing the entire screen element in liquid, draining the liquid, and pressuring the element with gas until bubble breakthrough. This method is used to test start baskets and traps, which are used for holding small amounts of liquid within the tank for engine restart.

A rigorous review of the literature revealed a total of 10 relevant studies of warm pressurant gas effects on LAD performance. LAD performance is affected by the surface tension, and, thus temperature. Therefore to make meaningful comparisons, historical results are organized by propellant type (function of saturation temperature), and then by screen type. A brief overview of historical results is presented chronologically.

Castle [26] first attempted to quantify the effect of heated pressurant on screen channel LAD performance. Using a standard NIBP configuration, they reported static bubble point tests conducted in LN₂ using GN₂ for six different

screen samples. GN_2 was heated electrically and forced downward on the LAD screen using a fan in an attempt to eliminate natural convection in favor of forced convection. For a $\Delta T = 50\text{K}$ across the screen, there was no degradation in performance for any screen mesh. Only the 250x600 mesh screen showed a 31% degradation in performance at a $\Delta T = 250\text{K}$.

Burge and Blackmon [7] reported heated gas LH_2 bubble points using a similar NIBP configuration as Castle [26] for three different meshes using GH_2 as a pressurant. A fan forced hot GH_2 down on the screen, but no attempt was made to eliminate natural convection. Results show performance degradation for all of the screens tested, with the finer 250x1370 mesh performing much worse than the coarser 200x600 mesh. The 250 mesh degraded to 30% of the cold gas breakdown point. Burge and Blackmon [7] also reported premature breakdown for a 200x1400 mesh with GH_2/LH_2 of 50% but did not report the gas temperature at breakdown. Due to the existence of both natural and forced convection, the screen likely broke down prematurely for all these tests. In addition, results are complicated by the fact that the liquid may have been subcooled relative to the pressurant gas temperature.

Paynter et al. [27] then conducted the first set of IO tests in LH_2 using both GHe and GH_2 . Test conditions were not reported, but Paynter reported no premature breakdown with warm gas under steady continuous outflow conditions, but premature breakdown for stepped or ramped expulsions. Blackmon [28] later conducted IO tests for a 250x1370 mesh in LH_2 using warm GHe and GH_2 . Results indicate a degradation in LAD performance as low as 75% at a $\Delta T = 35\text{K}$. Building on Paynter's tests, Warren [29] and Warren et al. [30] report IO data using two layers of 325x2300 screen mesh in LH_2 using both warm GHe and GH_2 . Neither saw premature LAD breakdown for continuous or stepped expulsion for a $\Delta T = 19 - 291\text{K}$.

Cady [25] reported NIBP test data for a standard 325x2300 screen, a pleated 325x2300, a stainless steel (SS) and aluminum (Al) 200x1400 screen, a 720x140, 165x800, and a SS and Al 120x120 screen in LH_2 using warm GHe . There is degradation in heated bubble point values for all meshes tested, with the largest reduction in performance for the 200x1400 screen. On average there was greater than 10% reduction in bubble point for temperature differences between gas and liquid as high as $\Delta T = 55\text{K}$. When compared to other heated gas 325x2300 LAD data, the data follows the general trend. Cady saw no difference between pleated and unpleated screen performance and saw no difference in performance between SS and Al screens. Examination of the test apparatus however showed that there was a direct view factor between heating source and screen. Therefore results here are complicated by the fact that heat was being conducted into the pressurant gas and also into the screen itself, which may have caused early breakdown. In addition, it is difficult to compare results from this NIBP configuration where only natural convection was present with those from Castle [26] where forced convection is dominant with Burge and Blackmon [7] where forced and natural convection were present.

Wilson and Meserole [31] report the first known heated pressurant gas LAD performance data using the IBP test configuration for a 325x2300 screen using GN_2 in IPA. They reported a reduction in performance of 69% of the cold gas bubble point at a $\Delta T = 56\text{K}$. But this data may also be corrupted due to the presence of a direct view factor between heat source and screen; the screen may have broken down early due to additional radiation heat transfer.

Bennett [32] tested the liquid retention capability of a 34 cm tall 250x1400 start basket with a 200x1400 window in LH_2 using both non-condensable and autogenous pressurization schemes. Here the basket was submerged in liquid into a dewar, the liquid level lowered below the basket, and warm pressurant gas was introduced until the basket ingested vapor. With GHe pressurant, no degradation in performance was noted, even when the LAD was subjected to GHe 70K above the liquid temperature. Using GH_2 pressurant however, results were not repeatable as the start basket broke down at a height of 0, 70, and 90% of the cold gas height.

The most recent investigation was conducted by Meserole and Jones [24] for a 325x2300 screen in LH_2 using both GHe and GH_2 using an IO test configuration and using GN_2 in Freon in an IBP configuration. In the IBP case, GN_2 was heated inside a cup with a heating element that was blocked from the screen to prevent stray radiation between heat source and screen. Gas was heated en route to the screen, which was submerged in Freon. A 325x2300 double-Dutch perforated plate, double plate backed 325x2300, and a pleated screen sandwich (325x2300, 25x25, 325x2300) were tested. The double-Dutch and double plated samples did not improve screen retention, as bubble point pressure degraded to 57% and 67% of the cold gas values, respectively, for $\Delta T = 83\text{K}$ and 100K, respectively. The onset of degradation did not occur until the gas temperature had risen 40K above that of the liquid. The pleated sandwich also did not improve screen retention over a single 325x2300 screen, as warm gas bubble point degraded to 75% at a $\Delta T = 99\text{K}$.

Meserole and Jones [24] also tested a 325x2300 perforated plate sample in LH_2 in a modified version of the test apparatus used in the Freon tests, in the IO configuration, and also in hold tests where liquid outflow was stopped for a period of time to allow sufficient residence time of the warm gas inside the dewar that held the LAD channel. IO test results used GHe , para- GH_2 , and normal GH_2 as pressurants. The trends are obvious; for GHe , for a ΔT as high as 62K, there was insignificant degradation (less than 5% reduction in performance). For hold tests with warm

GHe, there was no change in performance. For normal GH₂ pressurization, only a 6% reduction in performance was reported for a $\Delta T = 54K$ during continuous expulsion tests; for stepped expulsion tests, the LAD broke down at a height of 19% of the cold gas height when the GH₂ was only 5K above the liquid temperature. For para-GH₂ outflow tests, the LAD broke down at a height of 40% of the cold gas value at a $\Delta T = 26K$; for hold tests, the LAD broke down at a height of 19% of the cold gas height for a $\Delta T = 6K$.

Although trends from Meserole and Jones [24] are fairly obvious, in that GHe performed much better than GH₂ for both IBP and IO test configurations, the results are not repeatable and are complicated by the following reasons. First, the LAD itself was not sized properly. The hydrostatic head pressure inside the LAD when the LAD was completely exposed to gas was never enough to overcome the static bubble point pressure. As a result of the poorly sized LAD, a flow restriction orifice was used on the LH₂ inflow to help build up additional pressure differential. LAD breakdown was actually induced through the use of this flow restriction at the bottom of the tank by ramping the ullage pressure while still flowing through the flow restriction. The liquid level always dropped below the bottom of the LAD screen and breakdown only occurred when ramping the ullage pressure. It is unclear what the flow rate was during this pressurization event, and this is an indirect (and not direct) way to break the channel down. Second, warm gas was always injected at a temperature much greater than the actual temperature of the gas at the screen at breakthrough. Without direct measure of the temperature at the screen, it is unclear what the actual gas temperature was at the screen at breakdown. Third, for IO tests, a curved LAD was used, which only serves to complicate interpretation of results due to nonuniform flow-through-screen pressure losses. Fourth, while GHe and para-H₂ tests were fairly repeatable, there is quite a large discrepancy between para-GH₂ and normal GH₂ results, despite the fact that there is only a 1-2% increase in surface tension for para over normal hydrogen.

In summary, past inverted outflow tests are not ideal for assessing the fundamental effect of warm pressurant gas on LAD performance due to complexities in reducing the data, in controlling pressurant gas flow, and in controlling uniformity of the gas temperature. Dynamic IO tests are more flight representative than the simple static screen sample tests because the IO tests simulate 1-g outflow through a LAD channel from a larger propellant tank. However, for IO outflow tests, it is extremely difficult to control the location and direction of pressurization and also the uniformity of the temperature of the warm gas inside the tank relative to the LAD; even small changes in the direction or temperature of the gas can cause noticeable differences in the breakdown height of the channel as is shown in the historical data. The NIBP configuration is also not preferred due to complexities in controlling pressurant gas temperature and controlling gas flow down on the screen (i.e. natural vs. forced convection). Meanwhile, the IBP configuration is well suited to address this effect provided that careful attempts are made to heat only the gas, and not the screen. Care must also be taken to assure uniformity of temperature rise and to precisely measure the temperature of the pressurant gas before incidence on the screen. IBP configurations are preferred over IO configurations because it is better to heat the gas, then have the gas incident on the screen rather than warm the ullage space inside a large tank and then allow it to cool as it comes in contact with the LAD. Most discrepancies in previously reported experiments are due to these aforementioned concerns which can be mitigated through the new IBP experimental design presented in the current work.

References

- ¹McLean, C., Mustafi, S., Walls, L., Pitchford, B., Wollen, M., and Schmidt, J., "Simple, Robust Cryogenic Propellant Depot for Near Term Applications" *2011 IEEE Aerospace Conference*, Big Sky, MT, March, 2011.
- ²Fester, D.A., Villars, A.J., and Uney, P.E., "Surface Tension Propellant Acquisition System Technology for Space Shuttle Reaction Control Tanks" AIAA Paper 75-1196, *AIAA/SAE Propulsion Conference*, Anaheim, CA, September, 1975.
- ³Peterson, R. and Uney, P., "Development and Qualification of the Space Shuttle Orbiter Reaction Control System Propellant Tank" AIAA Paper 78-1026, *AIAA/SAE Joint Propulsion Conference*, Las Vegas, NV, July, 1978.
- ⁴Schweickert, T.F., "Design of the Aft Propulsion Subsystem for Long Life" *JANNAF Propulsion Meeting*, New Orleans, May, 1981.
- ⁵Anglim, D.D., "Space Shuttle Aft Propulsion Subsystem" AIAA Paper 81-1511, 1981.
- ⁶Anderson, J.E., "Superfluid Helium Acquisition System Development" *Cryogenics* Vol. 29, No. 5, 1989, pp. 513 – 516.
- ⁷Burge, G.W. and Blackmon, J.B., "Study and Design of Cryogenic Propellant Acquisition Systems – Volume II – Supporting Experimental Program" *NAS8-27685 MDAC Report MDC G5038*, 1973.
- ⁸Burge, G.W., Blackmon, J.B., and Castle, J.N., "Design of Propellant Acquisition Systems for Advanced Cryogenic Space Propulsion Systems" *AIAA/SAE Propulsion Conference* Las Vegas, NV, November, 1973.
- ⁹Zimmerli, G. A., Asipauskas, M., and Van Dresar, N. T., "Empirical correlations for the solubility of pressurant gases in cryogenic propellants," *Cryogenics*, Vol. 50, No. 9, 2010, pp. 556-560.
- ¹⁰Stiegemeier, B., Williams, G., Melcher, J.C., and Robinson, J., "Altitude Testing of an Ascent Stage LOX/Methane Main Engine" *5th JANNAF Liquid Propulsion Subcommittee Meeting*, May, 2010.

- ¹¹Hartwig, J.W., and Mann, J.A., “A Predictive Bubble Point Pressure Model for Porous LAD Screens” *Journal of Porous Media* (in press). 2014.
- ¹²Hartwig, J.W. and Mann, J.A., “Bubble Point Pressures of Binary Methanol/Water Mixtures” *AIChE Journal* Vol. 60, No. 2, 2014, pp. 730 – 739.
- ¹³Hartwig, J.W., Mann, J.A., Darr, S.R., and Chato, D.J., “Parametric Analysis of the Liquid Hydrogen and Nitrogen Bubble Point Pressure for Cryogenic Liquid Acquisition Devices” *Cryogenics* (accepted for publication) 2014.
- ¹⁴Hartwig, J.W., McQuillen, J.B., and Chato, D.J., “Screen Channel LAD Bubble Point Tests in Liquid Hydrogen” *International Journal of Hydrogen Energy* Vol. 39, No. 1, 2014, pp. 853 – 861.
- ¹⁵Jurns, J.M. and McQuillen, J.B., “Liquid Acquisition Device Testing with Sub-cooled Liquid Oxygen” AIAA Paper 2008-4943, Joint Propulsion Conference and Exhibit, Hartford, CT, July, 2008.
- ¹⁶Hartwig, J.W., McQuillen, J.B., and Chato, D.J., “Performance Gains of Propellant Management Devices for Liquid Hydrogen Depots” AIAA Paper 2013-0368, *Aerospace Sciences Meeting*, Grapevine, TX, January, 2013.
- ¹⁷Hartwig, J.W. and McQuillen, J., “Analysis of Screen Channel LAD Bubble Point Tests in Liquid Oxygen at Elevated Temperature” AIAA Paper 2011-3775, *Thermophysics Conference*, Honolulu, HI, June, 2011.
- ¹⁸Hartwig, J.W. and McQuillen, J., “Analysis of Screen Channel LAD Bubble Point Tests in Liquid Methane at Elevated Temperature” AIAA Paper 2012-0759, *Aerospace Sciences Meeting*, Nashville, TN, January, 2012.
- ¹⁹Hartwig, J.W. and McQuillen, J., “Screen Channel LAD Bubble Point Tests in Liquid Methane” *Journal of Thermophysics and Heat Transfer* (accepted for publication). 2014.
- ²⁰Hartwig, J.W., McQuillen, J., and Jurns, J., “Screen Channel LAD Bubble Point Tests in Liquid Oxygen” *Journal of Thermophysics and Heat Transfer* (accepted for publication). 2014.
- ²¹Hartwig, J.W. “Liquid Acquisition Devices for Advanced In-Space Cryogenic Propulsion Systems” *Dissertation*, Case Western Reserve University, Cleveland OH, May, 2014.
- ²²Hartwig, J.W. and Darr, S.R. “Influential Factors for Liquid Acquisition Device Screen Selection for Cryogenic Propulsion Systems” *Applied Thermal Engineering* Vol. 66, No. 1-2, 548 – 562. 2014.
- ²³Li, C. and Peterson, G.P., “The Effective Thermal Conductivity of Wire Screen” *International Journal of Heat and Mass Transfer* Vol. 49, No. 21-22, 2006, pp. 4095 – 4105.
- ²⁴Messerole, J.S. and Jones, O.S., “Pressurant Effects on Cryogenic Liquid Acquisition Devices” *Journal of Spacecraft and Rockets* Vol. 30, No. 2, 1993, pp. 236 – 243.
- ²⁵Cady, E.C., “Design and Evaluation of Thermodynamic Vent/Screen Baffle Cryogenic Storage System,” NASA-CR-134810, 1975.
- ²⁶Castle, J.N., “Heat Transfer Effects on Bubble Point Tests in Liquid Nitrogen” MDC02653, 1972.
- ²⁷Paynter, H.L., “Acquisition/Expulsion System for Earth Orbital Propulsion System Study, Volume II” NASA-CR-134154, 1973.
- ²⁸Blackmon, J.B., “Design, Fabrication, Assembly, and Test of a Liquid Hydrogen Acquisition Subsystem” NASA-CR-120447, 1974.
- ²⁹Warren, R.P., “Acquisition System Environmental Effects Study” NASA-CR-120768. 1975.
- ³⁰Warren, R.P., Butz, J.R., and Maytum, C.D. “Measurements of Capillary System Degradation” AIAA Paper 75-1197.
- ³¹Wilson, A.C. and Messerole, J.S., “Liquid Hydrogen Acquisition Device Component Fabrication and Testing” *D180-29345-1*. 1986.
- ³²Bennett, F.O., “Design and Demonstrate the Performance of Cryogenic Components Representative of Space Vehicles, Start Basket Liquid Acquisition Device Performance Analysis” NASA-CR-179138. 1987.